AD-A134 195 QUANTITATIVE SECONDARY ION MASS SPECTROSCOPY(U) 1/1
GEO-CENTERS INC NEWTON UPPER FALLS MA JUL 83
GC-TR-83-269 N00014-82-C-2099

UNCLASSIFIED F/G 20/12 NL

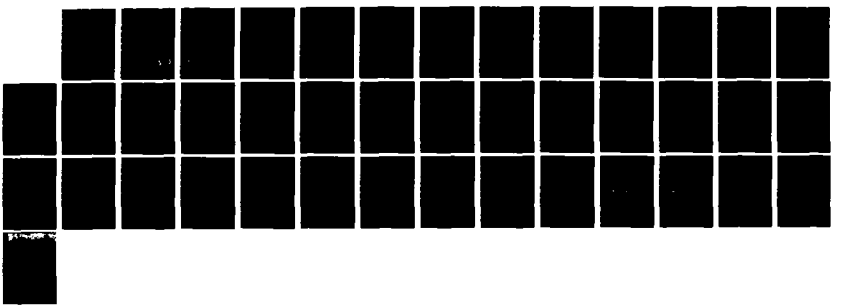

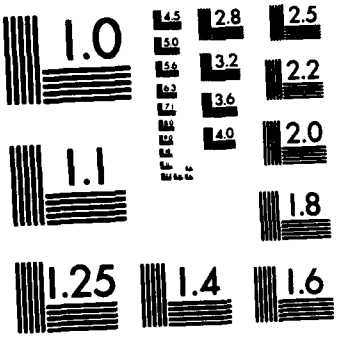

(10)

GC-TR-83-269

QUANTITATIVE SECONDARY ION MASS SPECTROSCOPY

GEO-CENTERS, INC.

(10)

GC-TR-83-269

QUANTITATIVE SECONDARY ION

MASS SPECTROSCOPY

PREPARED FOR
U.S. NAVAL RESEARCH LABORATORY
4555 OVERLOOK AVENUE
WASHINGTON, D.C. 20375
CONTRACT NUMBER N00014-82-C-2099

PREPARED BY
GEO-CENTERS, INC.
320 NEEDHAM STREET
NEWTON UPPER FALLS, MA 02164

JULY 1983

GEO-CENTERS, INC.

TABLE OF CONTENTS

FIGURE CAPTIONS

Figures 1 and 2. SIMS profiles of Be in GaAs at a Be concentration of $1.26 \times 10^{19}/cm^3$.

Figures 3 and 4. SIMS profiles of Be in GaAs at a Be concentration of $1.2 \times 10^{18}/cm^3$.

Figures 5 and 6. SIMS profiles of Be in GaAs at a Be concentration of $1.6 \times 10^{17}/cm^3$.

Figure 7. Measured SIMS intensity of Be^+ vs. Be concentration.

Figure 8. Schematic representation of Be concentration as a function of depth for a layered sample.

Figure 9. SIMS profile of layered sample represented in Figure 8.

Figure 10. SIMS profile for GaAs doped with Si ($3.3 \times 10^{18}/cm^3$) uniform to a depth of 0.75 microns.

Figure 11. Positive secondary ion spectra from 18Cr8Ni steel substrates obtained with 5.5 keV O_2^+ beam at current density J: (a) Ti-implanted in partial pressure of ^{13}CO gas ($J=200\mu A/cm^2$); (b) Ti-implanted in normal vacuum; ($J=90\mu A/cm^2$); (c) nonimplanted ($J=90\mu A/cm^2$).

FIGURE CAPTIONS (Continued)

Figure 12. Positive secondary ion spectra from Ni-plated substrates (at $J=220\mu A/cm^2$) implanted with Ti ions: (a) in partial pressure of ^{13}CO gas; (b) in normal vacuum.

Figure 13. Auger depth profile of 18Cr8Ni steel implanted with Ti^+ in the presence of ^{13}CO gas. Note change in sputtering current densities from $J=5\mu A/cm^2$ initially to $J=30\mu A/cm^2$ beyond the metal/oxide interface.

ACKNOWLEDGMENTS

We thank Bob Olfky and Randy Walker for assisting with the implantation; Dave Baldwin and Wayne Rabalais for discussion about streaming contamination; and Jim Comas and William Schmidt for providing samples of Be-doped GaAs and helpful discussions.

I. INTRODUCTION

This report describes in detail the use of the Cameca IMS-300 ion microscope for both quantitative analysis of sophisticated electronic devices and qualitative evaluation of ion implanted metals. The use of Secondary Ion Mass Spectroscopy (SIMS) in depth profiling adds a new dimension to surface analysis, enabling small concentrations of species which were previously undetectable to be determined. By being able to distinguish the differences in mass, isotopic techniques permit the elucidation of mechanisms which are responsible for the formation of wear resistant, low friction surfaces associated with titanium implantation into steels. The samples of semiconducting devices and ion implanted steels were provided to us by Naval Research Laboratory (NRL) personnel, but these evaluations by no means reflect the limits of versatility of this instrument.

An instrument so highly sophisticated is not without its own brand of maintenance problems. We have described both the maintenance and software modifications found necessary for efficient instrument operation.

II. QUANTITATIVE SECONDARY ION MASS SPECTROSCOPY

Surfaces of GaAs grown with known concentrations and distributions of Be and Si have been evaluated by SIMS. The results are hereby summarized, and are compared with the results of Leta and Morrison (1). The results which are described here show that the Cameca is operating at the same sensitivity as it was when located at Cornell. Be layers (80 Å, $10^{19}/cm^3$) near the GaAs surface were easily recorded. The strong dependence of the Si^+ signal on oxygen, coupled with the high background at mass 28, appears to preclude SIMS analysis of narrow Si layers.

Useful Ion Yield Be in GaAs

The "useful ion yield" is the number of ions detected/number of atoms sputtered. Since the target area (defined by the field of view) A=250 μm; interface depth, D_i; and Be concentration C; are known (Table 1), the number of Be atoms sputtered is simply

$$N_{Be} = A\ D_i\ C$$

Table 1. MBE Growth Data Supplied by Comas and Schmidt.

Sample	Be Concentration, C	Interface Depth, D_i
#29	$1.26 \times 10^{19}/cm^3$	2.5×10^{-4} cm
#32	$1.2 \times 10^{18}/cm^3$	2.5×10^{-4} cm
#33	$1.6 \times 10^{17}/cm^3$	2.0×10^{-4} cm

For constant Be^+ secondary ion signals the total number of Be^+ ions detected is the Be^+ signal/time, I^+_{Be}, multiplied by the sputter time, T, to the interface

$$N^+_{Be} = I^+_{Be}\ T$$

Table 2 contains the calculated useful ion yields, $\tau^+ = N^+/N$, for the six data files plotted in Figures 1-6.

Two SIMS data files were taken for each sample. For each SIMS run Be^+ and As^+ ions were recorded as a function of sputter time. As seen in Figures 1-6, the Be^+ ion signal remained relatively constant until it dropped sharply at the GaAs substrate interface. The depth of the interface given by Comas is listed in Table 1.

The calculated useful ion yields ranged from $5.4\text{x}10^{-7}$ to $5.3\text{x}10^{-6}$. The value given by Leta and Morrison (1) for Be in GaAs is $5\text{x}10^{-6}$. Also note that for data file #6 our Be^+ secondary ion (SI) signal is $\sim 10^2$ cps for $1.6\text{x}10^{17}$ Be/cm^3. Using 10 cps as our minimum count rate gives a detection limit for Be of $1.6\text{x}10^{16}$/cm^3 which is in agreement with results of Leta and Morrison.

Table 2.

Sample	Data File	I^+	Ti	N^+	N_{Be}	τ^+
#29	1	$1.0\text{x}10^3$	$1.9\text{x}10^3$	$1.9\text{x}10^6$	$1.26\text{x}10^{12}$	$1.5\text{x}10^{-6}$
	2	$7.5\text{x}10^2$	$9.1\text{x}10^2$	$6.8\text{x}10^5$	$1.26\text{x}10^{12}$	$5.4\text{x}10^{-7}$
#32	3	$2.6\text{x}10^2$	$1.8\text{x}10^3$	$4.7\text{x}10^5$	$1.2\text{x}10^{11}$	$3.9\text{x}10^{-6}$
	4	$7.4\text{x}10^1$	$1.0\text{x}10^3$	$7.4\text{x}10^4$	$1.2\text{x}10^{11}$	$6.2\text{x}10^{-7}$
#33	5	$4.2\text{x}10^1$	$6.9\text{x}10^2$	$2.9\text{x}10^4$	$1.3\text{x}10^{10}$	2.2x10-6
	6	$9.3\text{x}10^1$	$7.4\text{x}10^2$	$6.9\text{x}10^4$	$1.3\text{x}10^{10}$	$5.3\text{x}10^{-6}$

Sensitivity Factor for Be in GaAs

The instrumental parameters (focusing/transmission) are presumed to be the major factors in the variation of the useful ion yield. These factors are presumed to be largely mass independent so that sensitivity factors can be used to determine atomic concentrations. The sensitivity factor for Be in GaAs using As as the matrix signal is

$$S_{Be} = \frac{I_{Be}/C_{Be}}{I_{As}/C_{As}}$$

Using a density of 6 gm/cm^3 for GaAs gives an As concentration of $2.5 \times 10^{22}/cm^3$. Therefore, since $C_{Be} << C_{As}$ the presence of Be causes no variation in the bulk concentration of GaAs. Table 3 gives the sensitivity factors for the data files. The sensitivity factors are not constant but vary and give an average value of 36.4. Figure 7 plots the measured SIMS intensity of Be^+, I_{Be} (normalized to the As^+ matrix intensity at 2.5×10^5 cps), versus the Be concentration. Although the "measured" distribution is approximately linear (ignoring data file #2), it deviates from the "expected" curve which indicates one order of magnitude increase in Be signal intensity for each order of magnitude increase in Be concentration. The Cornell data point in Figure 7 correlates well with our data for $[Be]=1.2 \times 10^{18}$ cm^{-3}, and predicts a sensitivity factor of 30.9 for Be. Our data, however, deviates markedly from the expected curve at low (10^{17} cm^{-3}) and high (10^{19} cm^{-3}) Be concentrations. The measured deviation is attributed to either an unknown instrumental problem or to inaccuracies in the measured Be concentrations. We recommend that two ion implanted Be in GaAs with peak concentrations of $\sim 10^{17}$ and 10^{19} cm^{-3} be submitted for SIMS analysis to test for instrumental artifacts.

Table 3. Sensitivity Factors for Be in GaAs.

Sample	Data File	I_{Be}(cps)	$C_{Be}(cm^{-3})$	I^N_{Be}(cps)[a]	I_{As}(cps)	$C_{As}(cm^{-3})$	S_{Be}[b]
#29	1	1300	$1.26x10^{19}$	1800	$1.8x10^5$	$2.5x10^{22}$	13.9
	2[c]	630	$1.26x10^{19}$	280	$5.6x10^5$	$2.5x10^{22}$	2.3
#32	3	200	$1.2x10^{18}$	360	$1.4x10^5$	$2.5x10^{22}$	30.4
	4	80	$1.2x10^{18}$	320	$6.3x10^4$	$2.5x10^{22}$	26.8
#33	5	40	$1.6x10^{17}$	77	$1.3x10^5$	$2.5x10^{22}$	48.1
	6	100	$1.6x10^{17}$	100	$2.5x10^5$	$2.5x10^{22}$	63.0
Cornell[d]		310	$6.34x10^{17}$		$3.96x10^5$	$2.5x10^{22}$	30.9

[a] I^N_{Be} = normalized Be intensity when $I^N_{As} = 2.5x10^5$ cps.

[b] S = sensitivity factor = $(I_{Be}/C_{Be})/(I_{As}/C_{As})$.

[c] Data is questionable since the Be^+ ion signal did not increase (as the As^+ ion signal did) when the sputter rate was increased.

[d] Cornell result for ion implanted Be in GaAs, courtesy of George Ramseyer.

Sputter Rate of GaAs by O_2^+

The raster area used in all experiments was approximately 500μ x 500μ. For a 500μ x 500μ (0.25 mm^2) crater, the current density (in $\mu A/mm^2$) is four times the beam current. Table 4 lists the measured sputter rates for these samples.

Table 4.

Data File	Beam Current (μA)	Current Density ($\mu A/mm^2$)	Interface Depth d_i(Å)	Sputter Time t_i(sec)	Sputter Rate (Å/sec)
1	0.525	2.1	2.5×10^4	1890	13.2
2	1.0	4.0	2.5×10^4	910	27.5
3	0.525	2.1	2.5×10^4	1840	13.6
4	1.0	4.0	2.5×10^4	1025	24.4
5	1.0	4.0	2.0×10^4	700	28.6
6	1.0	4.0	2.0×10^4	740	27.0

Leta and Morrison's sputter rate for GaAs with a 1.0 μA O_2^+ ion beam and a crater area of .49 mm^2 is 19.1 Å/s. Our measured sputter rates for these MBE samples would be 12-14 Å/s with the sputtering conditions of Leta and Morrison.

Be Doped Layers

Figure 8 presents a schematic of the Be concentration as a function of depth for a layered sample. Note that the surface is to the right in this figure. The Be concentration of all Be layers is $10^{19}/cm^3$.

Figure 9 shows the SIMS depth profile of this sample. Some important points are:

(1) There are 12 peaks in the profile while Figure 8 suggests only 11;

(2) The counts/sec range from $\sim$2000 to $\sim$2900 for all implants with the wider implant regions recording higher counts;

(3) Based on points (1) and (2) above, the unlisted implant region appears to be 160 Å wide with a 330 Å gap;

(4) The plot places a symbol at every other data point;

(5) As was not monitored so the sensitivity factor cannot be determined;

(6) The useful ion yields for the first 80 Å layer is consistent with the previously determined τ^+ values, i.e.

$N_{Be} = 10^{19}/cm^3 \times (4\times10^{-4}\ cm^2) \times (8\times10^{-7}\ cm) = 3.2 \times 10^9$

Assuming $N_{Be}^+ \sim 2\times10^3$ gives τ^+ 2×10^{-6}.

Si in GaAs

Figure 10 shows the SIMS results for GaAs with doped Si ($3.3\times10^{18}/cm^3$) uniform to a depth of 0.75 microns. The decay of Si^+ signal results from the sputtering of surface oxygen. It is well known that the Si^+ ion yield is very dependent on oxygen coverage. The step at 0.75 microns is apparent. Although Leta and Morrison claim a detection limit for ^{28}Si in GaAs of 2×10^{20} (because of a large background 28 signal), we have measured an Si concentration of only $10^{18}\ cm^{-3}$. This measurement is possible

since the background signal in this sample is not too high, particularly beyond 0.4μ in depth. The oxygen dependency, however, suggests that SIMS depth profiling of thin Si layers might be difficult due to the influence of surface oxygen on the Si SI yield.

III. QUALITATIVE ANALYSIS

Secondary ion mass spectrometry has been used to analyze the surface composition of several steel and Ni-plated substrates implanted with Ti ions (5×10^{17} Ti/cm^2 at 190 keV). SIMS showed clearly the carbonaceous subsurface layer previously reported in Auger and Nuclear backscattering analyses of Ti-implanted Fe-based alloys. Moreover, substrates implanted in a vacuum which was backfilled with isotopic ^{13}CO gas showed 20 to 50 times higher mass 13/mass 12 ratios for surface concentrations and integrated subsurface doses than substrates implanted in normal vacuum atmospheres at pressures near 10^{-6} Torr.

Auger analysis confirmed the subsurface C profile and found no O (<1 at.%) below the oxide layer. The experiments provide direct evidence that C atoms can be absorbed from residual gas molecules in a vacuum chamber at near room temperatures during implantation of carbide-forming ions. A second possible source of C atoms is also discussed, and anomalies in the secondary ion yields from the carbonaceous layer are described.

Anomalously high concentrations ($\sim$20 at.%) of carbon have been detected in surfaces implanted to high fluences with carbide-forming metal ions (2-5). Auger depth profile (2,4,5) and non-destructive nuclear backscattering (3,6,7) analyses of Ti-implanted Fe-based alloys (the most extensively studied system) have revealed a diffusion-like profile of carbidic atoms in an

amorphous layer which grows inward with increasing fluence. These results have led investigators to speculate that carbon (C) is absorbed from the vacuum chamber during implantation. We report direct experimental evidence that excess C found in Ti-implanted alloys can originate from residual gas molecules in the implantation vacuum chamber.

The experiment consisted of implanting Ti into substrates exposed to a partical pressure of ^{13}CO gas, then detecting ^{13}C atoms in the implanted surface using secondary ion mass spectrometry (SIMS). The ^{13}C atoms are expected to pass from the gas phase ^{13}CO molecules to the solid surface by a process we call implant-assisted vacuum carburization (5). During implantation, incoming ions erode the surface and eventually uncover previously implanted Ti. At the surface, Ti atoms adsorb residual carbonaceous gas-molecules, which dissociate to form surface carbide species. These surface carbon atoms in turn diffuse or otherwise move inwards during continued implantation bombardment. CO gas was chosen for this experiment because it has a high probability of sticking to Ti at room temperature and dissociatively chemisorbs to form surface carbide species (8).

Implantation of Ti ions, in NRL's cryopumped Varian/Extrion implanter, is normally performed with the vacuum chamber at pressures from 1 to 4 x 10^{-6} Torr and at current densities of J$\sim$5 to 20$\mu A/cm^2$ (2,4). For the ^{13}C experiment, the vacuum chamber was pumped overnight and reached a base pressure of P=4 x 10^{-7} Torr. The pressure rose to P=6 x 10^{-7} Torr with the entry of a Ti ion beam at (J=10$\mu A/cm^2$), then to P=4 x 10^{-6} Torr as ^{13}CO gas was bled into the chamber. This pressure was maintained throughout the implantation period by a continuous flow of ^{13}CO gas.

The sample sets consisted of three polished steel substrates (a high carbon steel, a low carbon steel and an 18Cr8Ni steel (9))

and one Ni-plated substrate. Substrates were pasted to a water-cooled holder (to keep the temperature below 40°C) then implanted to a fluence of 5×10^{17} Ti/cm^2. One set was implanted with the ^{13}CO gas present, a second set at normal vacuum conditions (i.e. without ^{13}CO gas) and a third set remained non-implanted.

Composition vs. depth profiles of the implanted layer were obtained by Auger electron spectroscopy and Secondary Ion Mass Spectrometry (SIMS). Auger data were obtained during 2 KeV Ar-ion milling with a CMA analyzer with a 3 eV modulation voltage and a 2 kV electron beam voltage. SIMS data were acquired on a Cameca ion microscope (Model IMS-300) using a 5.5 keV O_2^+ primary ion beam. The beam was rastered over an area typically 0.6 mm x 0.9 mm at currents from 500 to 800 μA. The weak positive secondary ion signals of C and O required count times 100 times longer than the strong positive metal ion signals. All samples were sputtered cleaned for 15 seconds prior to counting to avoid the strong secondary ion peaks resulting from the contaminated oxide surface. The mass 12 intensity is taken to represent $^{12}C^+$ ions. The mass 13 intensity should be principally $^{13}C^+$, although some CH^+, also mass 13, may contribute due to the lack of UHV conditions in the SIMS vacuum chamber.

Figure 11 presents selected SIMS profiles for the 18Cr8Ni steel substrates. The C introduced into the surface by Ti implantation is clearly identified as the mass 12 and mass 13 intensities (i.e. ^{12}C and ^{13}C curves) in Figures 11(a) and (b); cross-hatched and dotted areas indicate the excess C above steady-state values. The excess C concentration found in the non-implanted substrates (Figure 11(c)) is quite small, albeit exaggerated by the logarithmic scale; it probably resulted from beam mixing of carbonaceous overlayers found on all surfaces. Both excess carbon curves, ^{12}C and ^{13}C, fall to steady-state

values with diffusion-like tails, consistent with Auger results (shown below). The steady state mass 13/mass 12 ratio, however, is less than one-half of the expected isotopic $^{13}C/^{12}C$ ratio (1:99); we believe that CH^+ may have contributed to the mass-13 intensity.

Figure 11(a) provides direct evidence for the adsorption of C from the gas phase. It shows a much greater proportion of ^{13}C than Figure 11(b) (the substrate implanted without ^{13}CO gas): the mass 13/mass 12 intensity ratio at the surface, approximately 1:1, is more than 30 times greater, and the integrated mass 13/mass 12 dose ratio is approximately 40 times greater. Similar ratio values were obtained from the two other steel samples.

The Ni substrates also had excess C after Ti implantation and enhanced mass 13/mass 12 ratios for the substrate implanted in the presence of ^{13}CO gas, as shown in Figure 12. There were, however, two differences in the spectra of Ti-implanted Ni and Ti-implanted steels. First, more excess C was found in the steels than in the Ni, despite identical implantation conditions and similar Ti concentration profiles. This difference, indicated by the mass 12 or mass 13/Ti mass 48 ratios in Figures 11 and 12, has also been verified by Auger composition vs. depth profiles (not shown). Vacuum carburization, however, is a complicated interplay of sputtering, chemisorption and diffusion (probably radiation-enhanced), and factors affecting the carburization rates of different metals are not understood. For example, Cr atoms on the 18Cr8Ni steel surface might provide a second site for C adsorption, thereby enhancing the C absorption rate. A second difference was that the mass 13/mass 12 ratio in the ^{13}CO-on-Ni substrate reached 3, but was never more than 1 for the CO-on-steel substrates.

One of the unanswered questions of the SIMS analysis is why the mass 13/mass 12 is not greater than observed. If the ^{13}CO gas

pressure was (as measured) seven times greater than the background pressure and ^{13}CO has a sticking coefficient as high as any other residual gas species (as expected), then the $^{13}C/^{12}C$ ratio should be at least 7:1. (We assume that the ionization yields of ^{12}C and ^{13}C are the same, and we verified that the gas bottle contained at least 99% ^{13}CO ratio.) One possible explanation for the lower ratio is that a large flux of neutral low energy contaminant molecules (e.g. CO, CO_2, CH_4) may have "streamed" along with the ion beam. A large increase in the local pressure at the target would be measured as a small increase in the overall chamber pressure; this "streaming" may account for the rise in background pressure from $4x10^{-7}$ Torr to $6x10^{-7}$ Torr when the Ti^+ beam was turned on.

The relative concentrations of C to O absorbed during Ti implantation in ^{13}CO gas were obtained from Auger depth profiles of the steel and Ni substrates. Figure 13 presents selected Auger depth profiles of the near surface region of the 18Cr8Ni steel analyzed in Figure 11(a). The surface oxide/metal interface was profiled slowly ($J=5\mu A/cm^2$) a 2 keV Ar^+ ion beam. The C signal rises to near maximum value at the oxide/metal interface, where the O signal from the oxide layer falls to negligible intensity (less than 1 at.% concentration). The remaining profile, taken at a faster rate ($J\sim30\mu A/cm^2$), shows C falling off with a diffusion-like tail and O never reappearing. Therefore, only the C, not the O is selectively absorbed during the implant-assisted vacuum carburization process.

The main finding of this experiment has been that excess carbon in the Ti-implanted surface originated from residual gases in the vacuum system. We have shown here that vacuum carburization can occur in Ni as well as Fe alloys, and the C but not O is absorbed. Recently, one of us (ILS) has reported that Cr and Ta implants also carburize metals and suggested that carburization

should occur for any strong carbide former implant to high fluences (5). Implant-assisted vacuum carburization is expected to occur so long as the attack rate of residual gases is greater than the sputtering rate by the ion beam. This hypothesis is now being tested at NRL by performing implantations at high dose rates in a UHV chamber, with and without ^{13}CO gas. These investigations should also reveal whether contaminant streaming contributes to implant assisted carburization in high vacuum.

IV. ION MICROSCOPE MAINTENANCE

The depth profiling ion microscope consists of two parts: (1) the Cameca IMS-300 and (2) the PDP-11/20 and GT-40 computer and associated electronic hardware. When the IMS-300 was obtained by Cornell, Cameca offered no computer system so that Cornell developed their own system. This system was based on a PDP-11/20 minicomputer and used other Digital Equipment Corporation (DEC) hardware in their system (e.g. a GT-40 graphics terminal with 11/05 processor). However, a non-standard parallel data transfer (PDT) line was constructed to enable rapid data display. The PDT was not serviceable by DEC which caused prolonged problems when the PDT failed. Also, NRL did not receive all the computer system components from Cornell. The line printer and data plotter were the most useful of this missing hardware. A Trilog T-100 Printer/ Plotter was purchased with the goal of replacing both missing components with a single unit. This substitution forced significant plotting software changes described in the Software Maintenance Section.

After the particle multiplier and preamp were serviced by Cameca so that the Cameca electron registered expected currents, it was still not possible to record these pulses on the computer. In tracing the multiplier signal to the computer, an output switching line was broken causing the apparent loss of computer function.

DEC servicemen worked on both the PDP-11/20 and 11/05 for several days. After finally locating the broken wire on the Cornell-made output select board, the computer system was shown to operate properly on various test programs. Still, the initiation of the PDT lines was not possible.

At this time the architect of the PDT system, James Roth, was hired as a consultant with two objectives: (1) correct the problem preventing use of the PDT line and (2) find the problem with the pulse counting circuit.

Upon Roth's arrival only 8K of memory could be addressed. This was enough to boot the system but PDT was not possible. Improper insertion of a GT-40 backplane card was found to be the problem. Proper insertion restored all memory addresses and PDT data transfer.

The pulse counting problem was then addressed. At this time the pulse counter recorded only a small fraction of the ion pulses. The ion pulses exhibited a high frequency "ringing" shape instead of the single 50 μs pulse expected. Connections and cables were examined and repaired from the preamp to the computer. This cable pathway was shortened and the expected pulse at the computer input was obtained, but still these pulses were not computer recorded.

The problem was internal to the computer. The ion pulse was input to board I0Ø8. The signals on this card were examined using an extender card for easier access. The input pulses were produced by a pulse generator. A line power transistor altered the input pulse shape. Replacing this transistor did not produce a pulse identical to the input. Finally, this transistor was

eliminated by using a previously unused inverting gate on this card. This resulted in good pulse shape and correct pulse counting.

After satisfying both of the initial objectives of his consultation, Roth assembled and explained the circuit diagrams pertaining to the PDT IO cards and noted which components are used on the current system configuration. The main data acquisition program was largely written by Roth. He was given copies of modules which were changed after his departure from Cornell. This will enable him to aid in future troubleshooting by telephone if modifications to this program are attempted.

No satisfactory answer exists for computer hardware problems. DEC service is expensive and unreliable if the problem can't be localized to the DEC section of hardware. The age of the system (1972) can result in servicemen unfamiliarity with the computer. James Roth retains all his knowledge of this system and his unparalleled expertise, but his availability to address future problems may prove problematic. Computer advances suggest that new, less expensive hardware could replace the current hardware when expensive repair becomes necessary. The implementation of a back-up microcomputer system should be explored.

V. COMPUTER SOFTWARE

Since a Trilog printer/plotter was purchased to replace the plotter used at Cornell, new plotting software was necessary. Cerritos software was purchased as a high level plotting language. Implementation of this software on the PDP-11/20 was slowed by 11/20 assembly language differences from more recent versions. This problem was eventually solved by writing a macro-routine to replace a machine language instruction.

Plotting with Cerritos is performed by generating an intermediary plot file using calls to plot subroutines in a Fortran plot program. A Cerritos conversion program then translates this intermediary file into the hard plot.

Drawbacks to using the Trilog device with Cerritos software for plotting are:

(1) Although the intermediary files are generated in less than one minute from a data file, the conversion program required at least five minutes to generate a plot.

(2) The size of Cerritos prevents its incorporation as a PROBE subroutine. This means that data must be stored and plots generated by separate programs afterwards.

(3) The Cerritos software is restrictive in that some desired plotting changes are very difficult to implement (for example, rotating the plot axes proves to be very difficult).

Plotting programs were written to output depth profile data. Briefly, these programs plot the ion intensities for each element in the data file versus a time dependent number. The data for each element is uniquely labelled and connected by a line. The intensities may be plotted linearly, logarithmically, or normalized to the maximum signal for each element. On the plot, the symbols used for all elements are identified along with the maximum reading for each element. The title and data file name is printed at the top of each plot. If the depth of the crater is measured after analysis, the time can be simply converted to depth of origin for plotting. Examples of these plotting program outputs are included in the Quantitative Applications Section.

A software project which was recently begun and remains unfinished was the redesign of the fundamental data acquisition program, PROBE. Dave Kidwell was the prime architect for this change. The Cornell Probe program requires intimate familiarity with the PROBE program and repeated reference to printed instructions with little prompting by the program. The objective in the new rewrite was to make PROBE more "user friendly." In this new version the user is presented with menus from which to select desired application. The parameters required are always entered from the keyboard in response to computer prompts to the user. Also, the data is stored as it is taken instead of after the data is acquired. This latter feature of the old program resulted in the loss of much data because of computer or user error in attempting to write the data to a storage file. Also, the old

data files reserved space for the maximum amount of data and filled the excess space with zeros if unused. The new system avoids all this wasted file disk space.

In conclusion, the computer software now works adequately, but improvement continues. The rewriting of the fundamental data acquisition program is nearly complete and will greatly simplify user interaction. Many of the old routines which were useful at Cornell were found non-appropriate at NRL and eliminated. Dave Kidwell is clearly the most knowledgeable person regarding the new software.

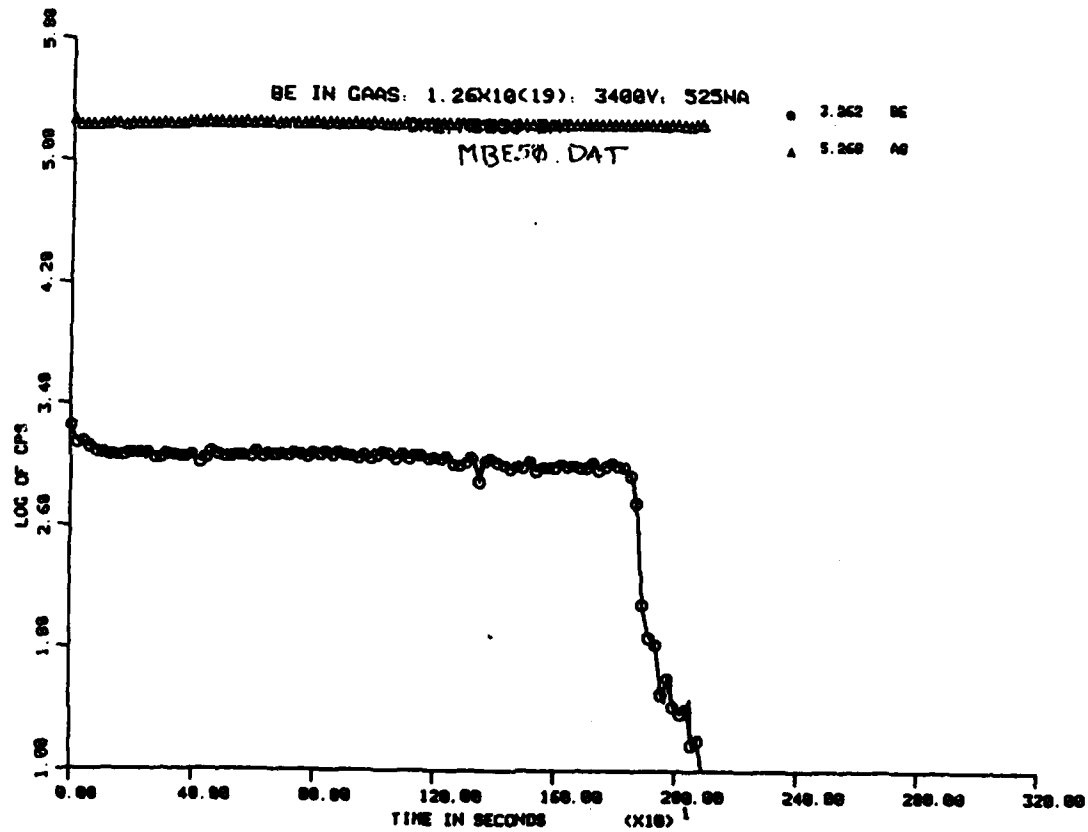
BE IN GAAS: 1.26X10(19): 3400V: 525NA
MBE50.DAT
LOG OF CPS
TIME IN SECONDS
(X10)

Figure 1

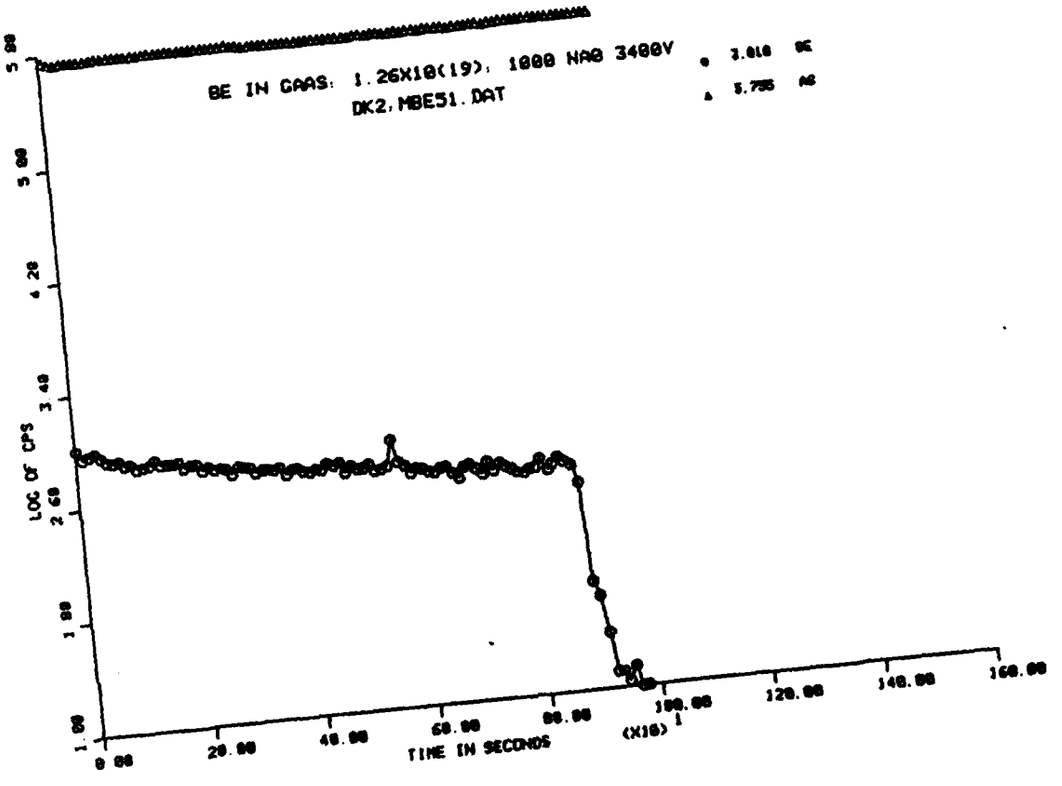
BE IN GAAS: 1.26X10(19): 1000 NAG 3400V
DK2.MBE51.DAT
LOG OF CPS
TIME IN SECONDS
(X10) 1

Figure 2

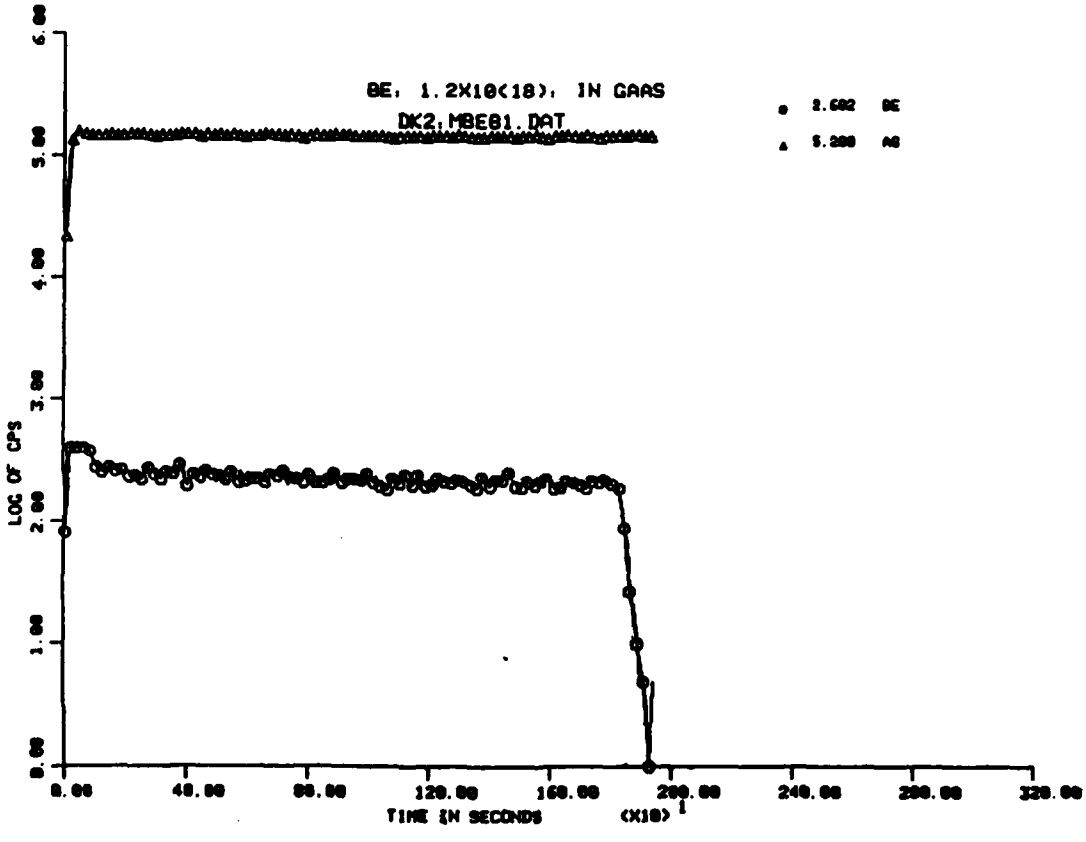
BE: 1.2X10(18): IN GAAS
DK2.MBE01.DAT
LOG OF CPS
TIME IN SECONDS
(X10)

Figure 3

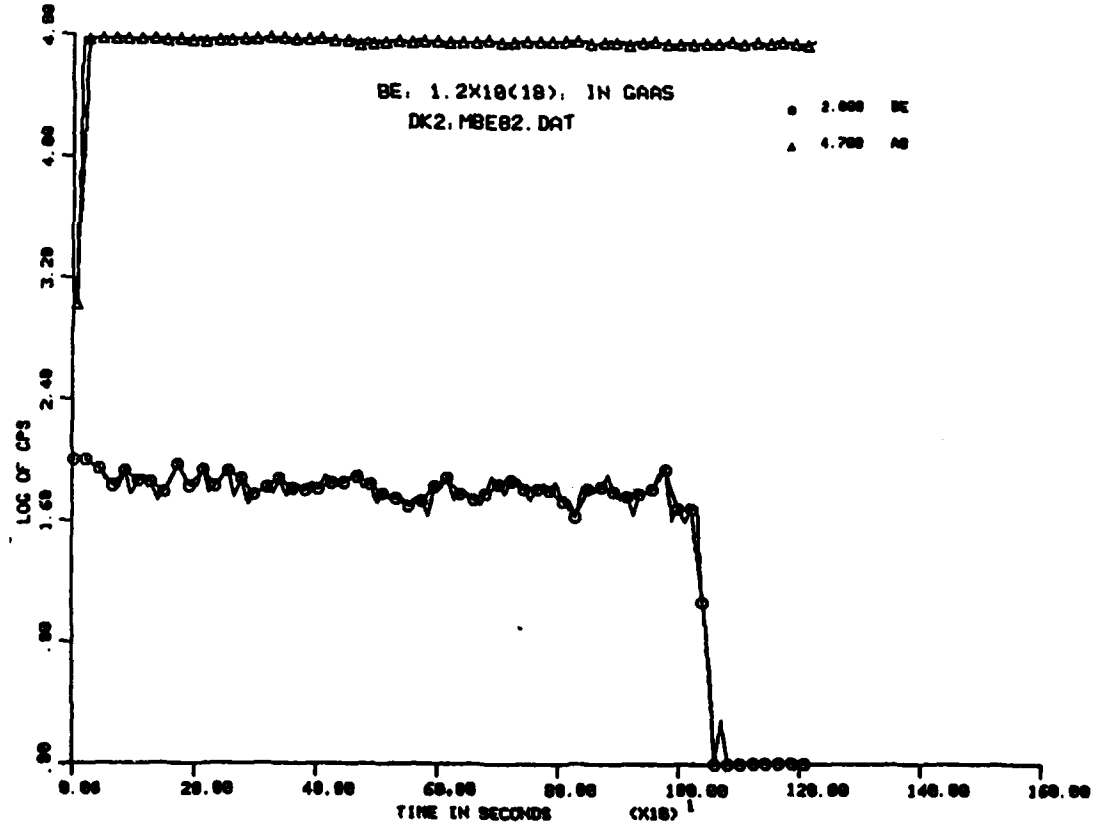
BE: 1.2X10(18): IN GAAS
DK2:MBE82.DAT
LOG OF CPS
TIME IN SECONDS
(X10)

Figure 4

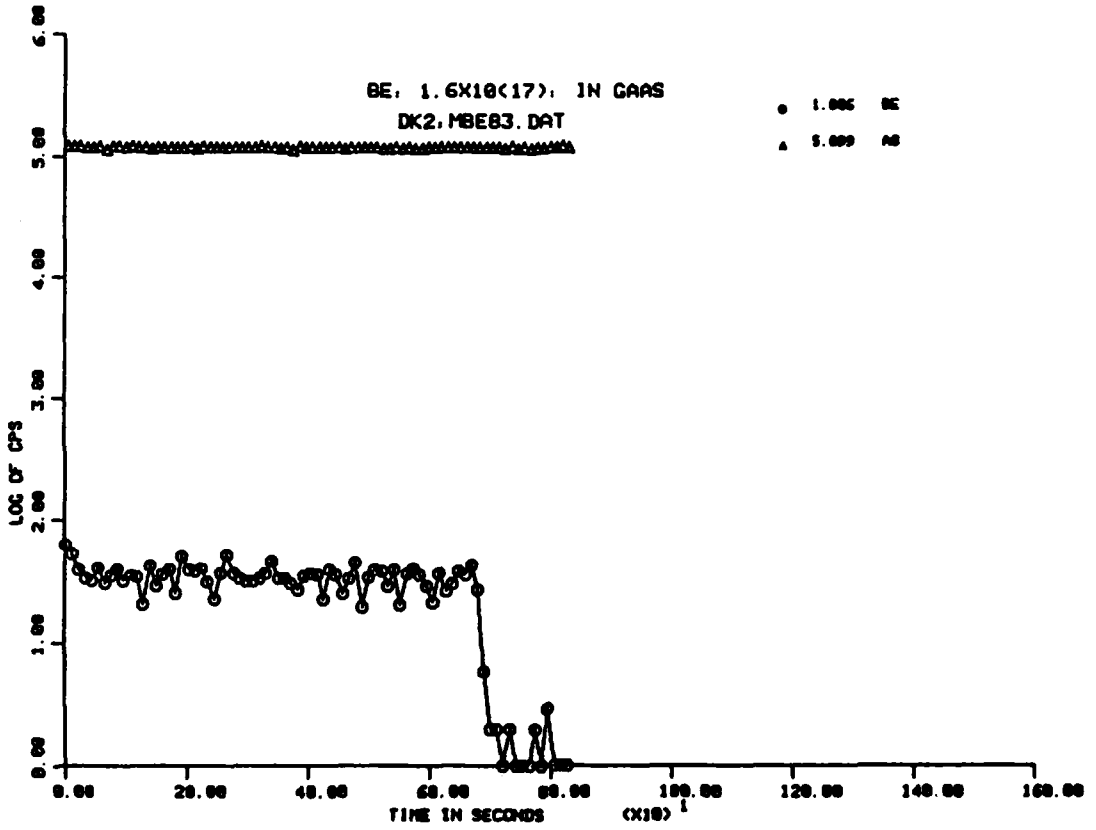
BE: 1.6X10(17): IN GAAS
DK2.MBE83.DAT
LOG OF CPS
TIME IN SECONDS
(X10)

Figure 5

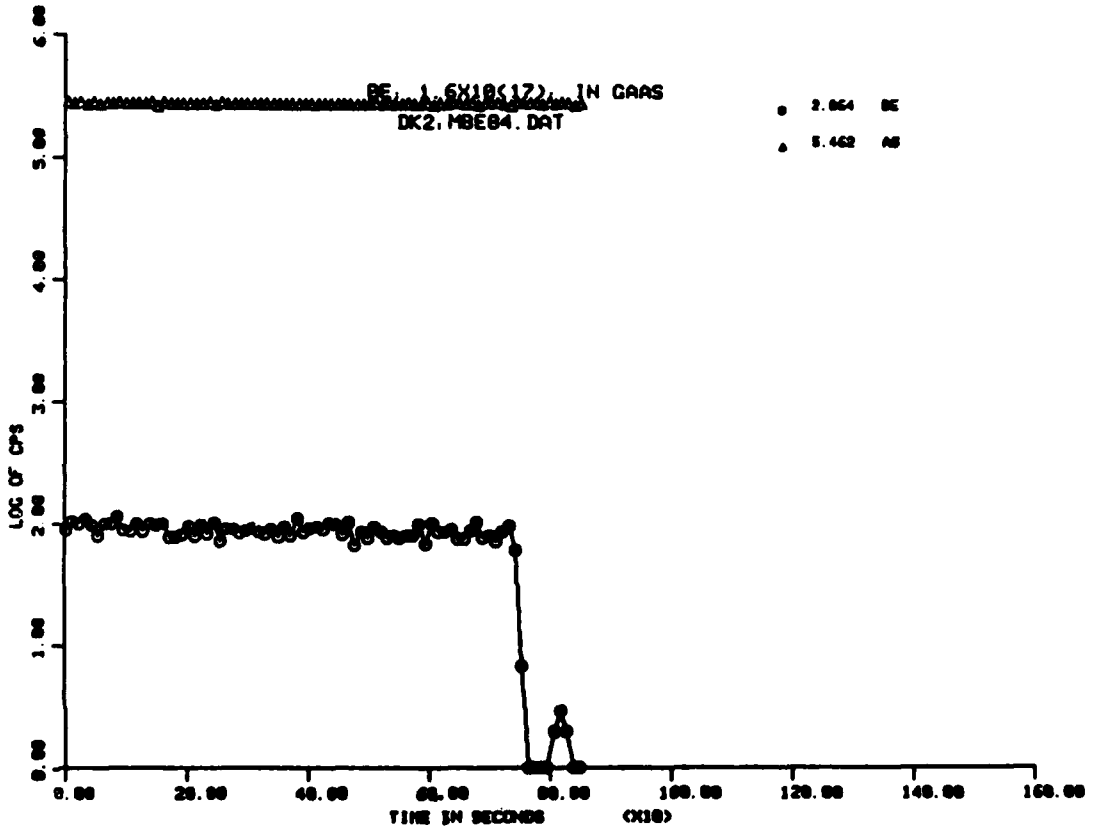
BE, 1.6X10(17), IN GAAS
DK2:MBE84.DAT
LOG OF CPS
TIME IN SECONDS
(X10)

Figure 6

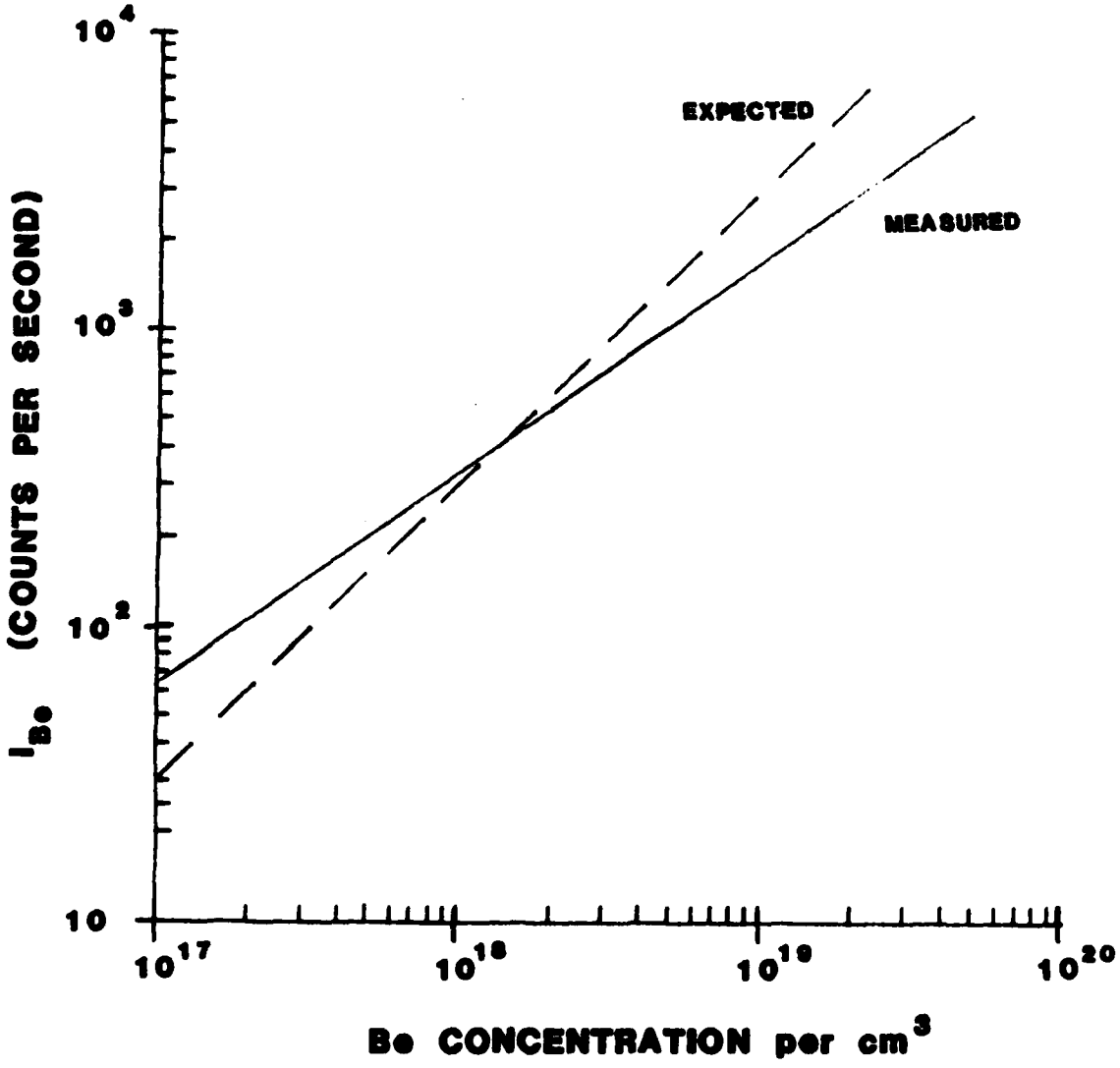
10^4
10^3
10^2
10
I_{Be} (COUNTS PER SECOND)
EXPECTED
MEASURED
10^{17}
10^{18}
10^{19}
10^{20}
Be CONCENTRATION per cm^3

Figure 7

MBE GaAs Be-DOPED LAYERS

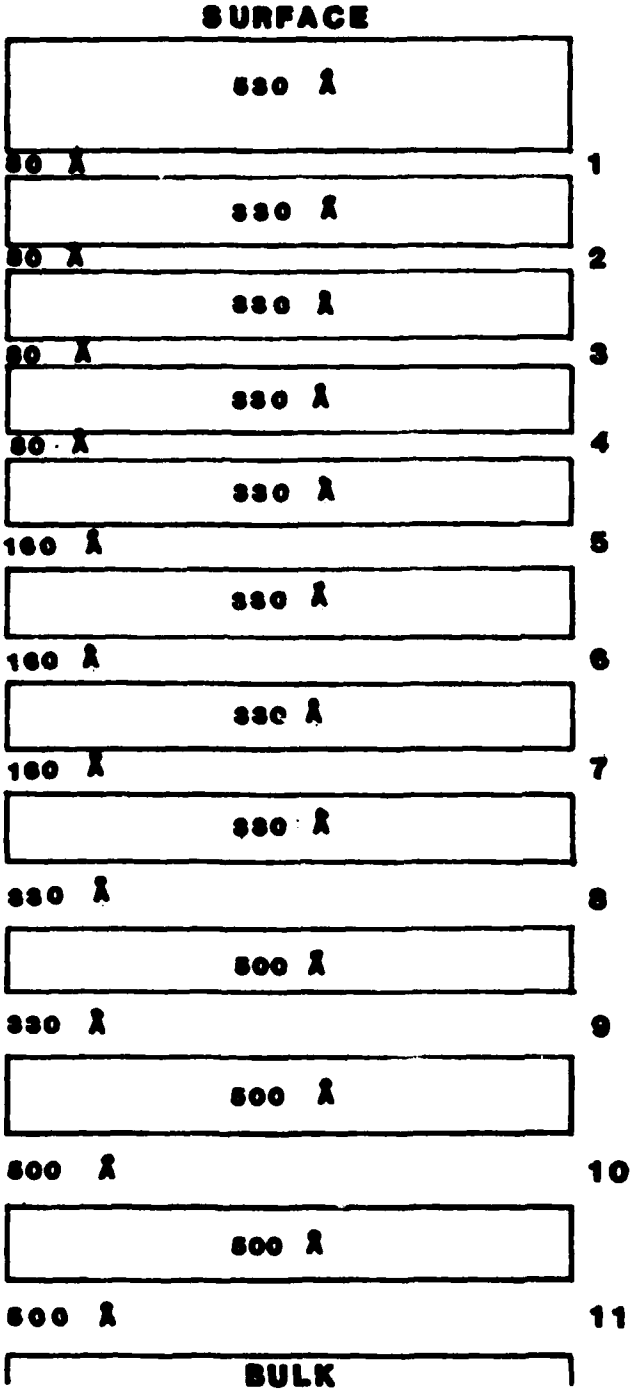

Figure 8

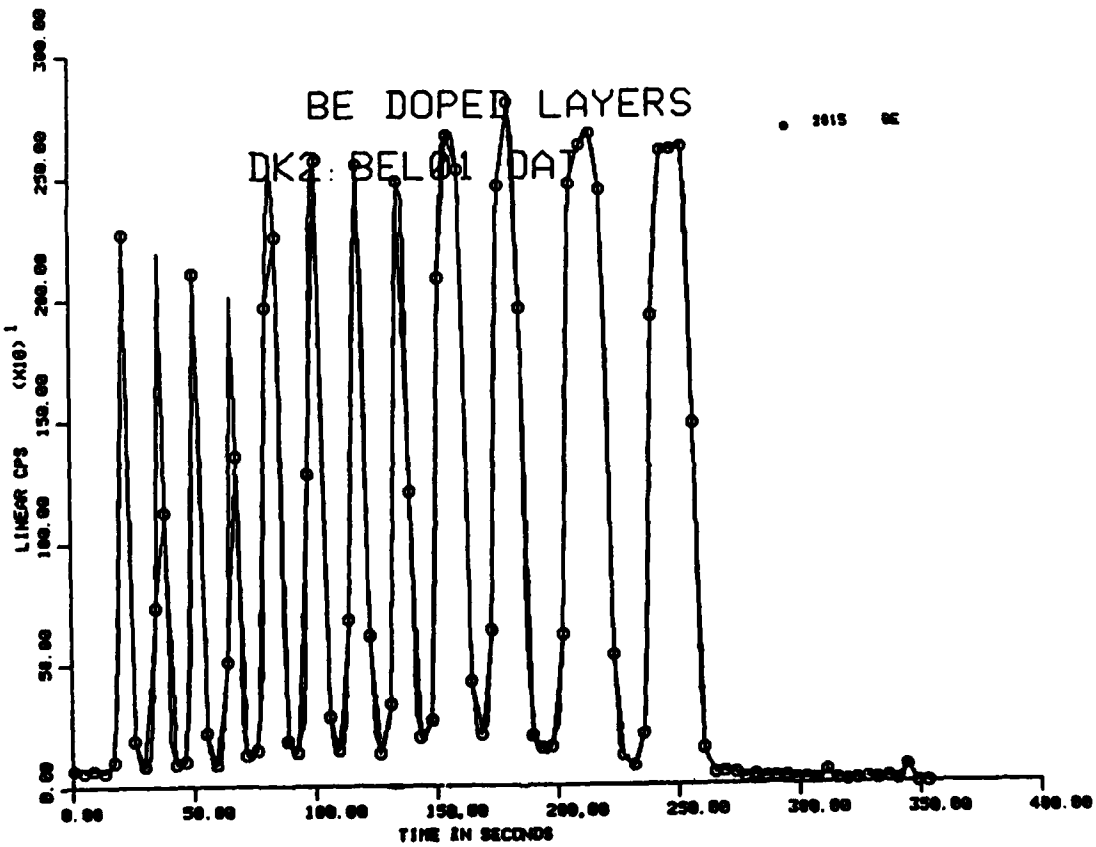
BE DOPED LAYERS
DK2:BEL01.DAT
LINEAR CPS (X10)
TIME IN SECONDS
0.00
50.00
100.00
150.00
200.00
250.00
300.00
350.00
400.00

Figure 9

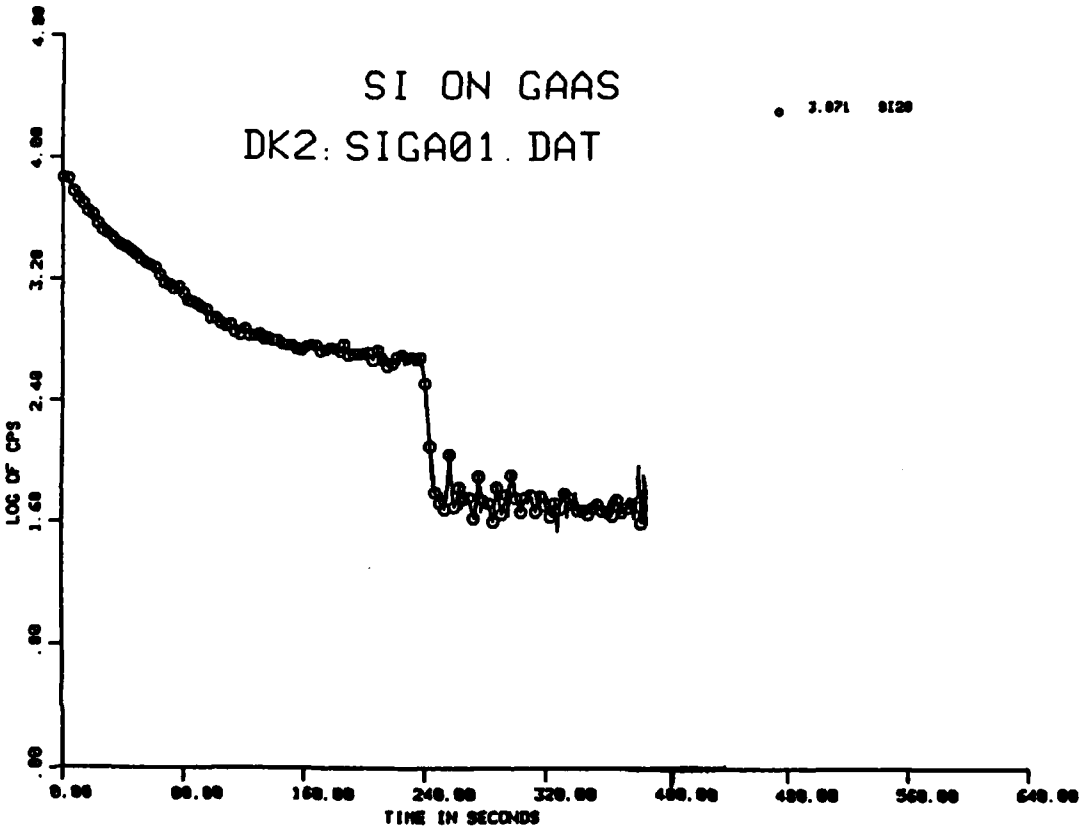

Figure 10

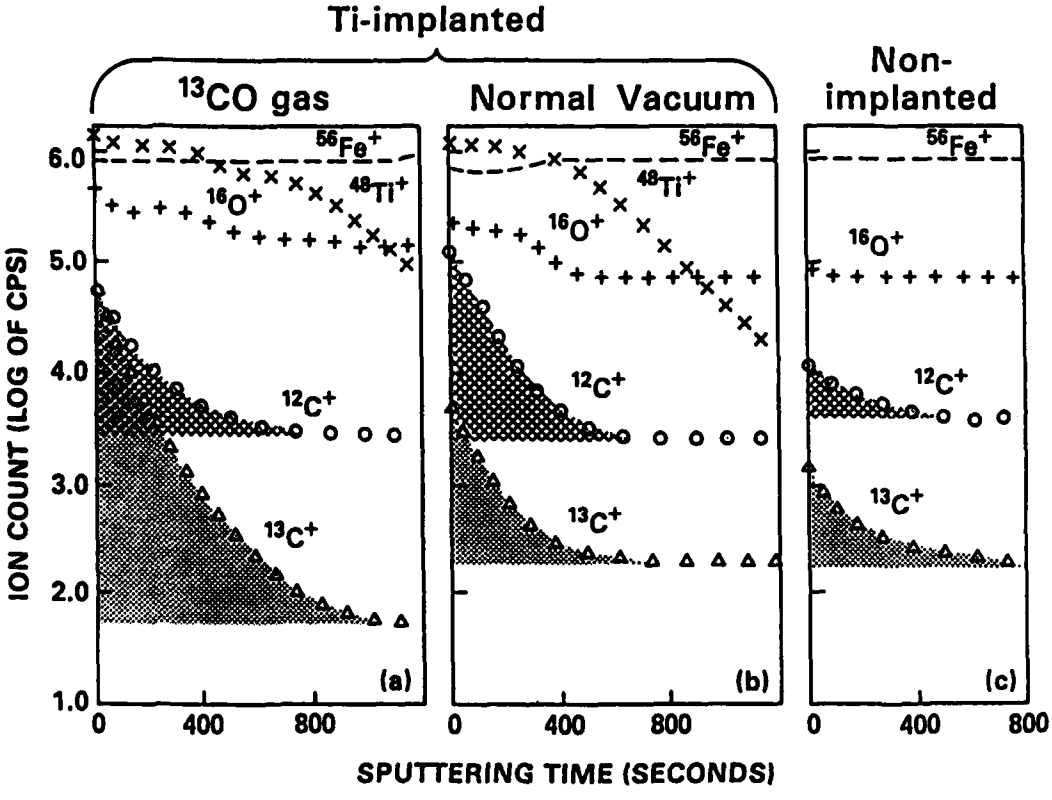
SIMS DEPTH PROFILE
Ti-implanted
^{13}CO gas
Normal Vacuum
Non-implanted
$^{56}Fe^+$
$^{48}Ti^+$
$^{16}O^+$
$^{12}C^+$
$^{13}C^+$
ION COUNT (LOG OF CPS)
6.0
5.0
4.0
3.0
2.0
1.0
0
400
800
(a)
(b)
(c)
SPUTTERING TIME (SECONDS)

Figure 11

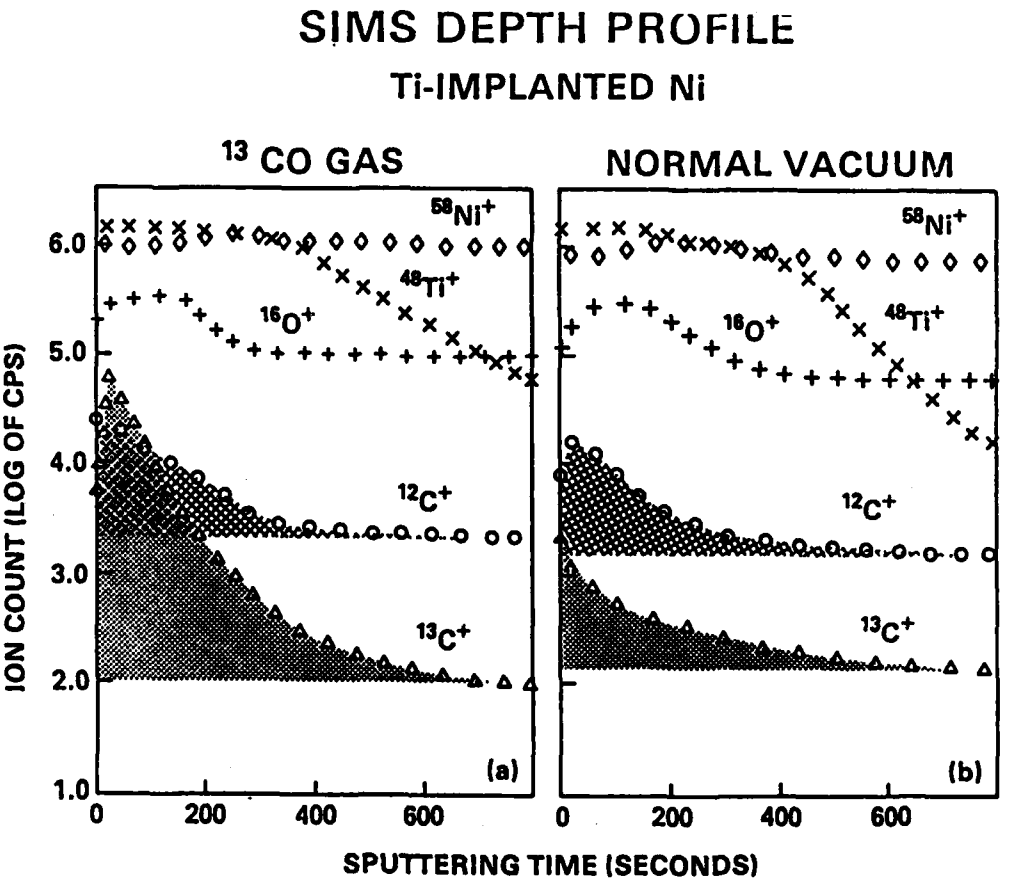
SIMS DEPTH PROFILE
Ti-IMPLANTED Ni
13 CO GAS
NORMAL VACUUM
58Ni+
48Ti+
16O+
12C+
13C+
(a)
(b)
ION COUNT (LOG OF CPS)
6.0
5.0
4.0
3.0
2.0
1.0
0
200
400
600
SPUTTERING TIME (SECONDS)

Figure 12

AUGER DEPTH PROFILE OF 304 STEEL IMPLANTED WITH Ti ($5 \times 10^{17}/cm^2$ AT 190 keV) IN PRESENCE OF ^{13}CO GAS ($p \sim 4 \times 10^{-6}$ Torr)

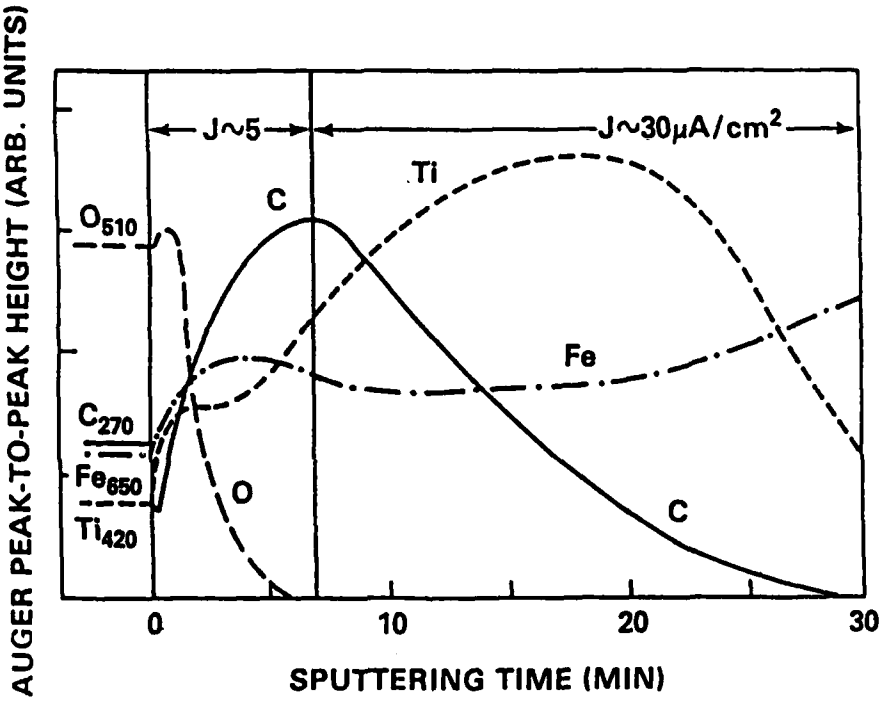

Figure 13

REFERENCES

1. D. Leta and G. Norrison, Analy. Chem., 52, 514 (1980).

2. C.A. Carosella, I.L. Singer, R.C. Bowers, and C.R. Gossett, in Ion Implantation Metallurgy, C.M. Preece and J.K. Hirvonen (editors) (Metallurgical Society of AIME, Warrendale, Pennsylvania, 1980), p. 103.

3. J.A. Knapp, D.M. Follstaedt, and S.T. Picraux, Appl. Phys. Lett., 37, 330 (1980); see also in Ion Implantation Metallurgy, C.M. Preece and J.K. Hirvonen (editors) (Metallurgical Society of AIME, Warrendale, Pennsylvania, 1980), p. 152.

4. I.L. Singer, C.A. Carosella, and J.R. Reed, Nucl. Instrum. and Meth., 182/183, 923 (1981).

5. I.L. Singer, J. Vac. Sci. Technol., Apr (1983).

6. C.R. Gossett, Nucl. Instrum. and Meth., 191, 335 (1981).

7. G.K. Hubler, Nucl. Instrum. and Meth., 191, 101 (1981).

8. M.P. Hooker and J.T. Grant, Surface Sci., 62, 21 (1977).

9. The high carbon steel was type 52100 (Fe1.5Cr1C); the low carbon steel was type 1018 (FeO.2C); the 18Cr8Ni steel was type 304 (Fe18Cr8NiO.06C) all given in wt.%.